No detection of methane on Mars from early ExoMars Trace Gas Orbiter observations

Oleg Korablev, Ann Carine Vandaele, Franck Montmessin, Anna A. Fedorova, Alexander Trokhimovskiy, François Forget, Franck Lefèvre, Frank Daerden, Ian R. Thomas, Loic Trompet, et al.

No detection of methane on Mars based on early ExoMars Trace Gas Orbiter observations

Oleg Korablev[1], Ann Carine Vandaele[2], Franck Montmessin[3], Anna A. Fedorova[1], Alexander Trokhimovskiy[1], Francois Forget[4], Franck Lefèvre[3], Frank Daerden[2], Ian R. Thomas[2], Loïc Trompet[2], Justin T. Erwin[2], Shohei Aoki[2], Séverine Robert[2], Lori Neary[2], Sébastien Viscardy[2], Alexey V. Grigoriev[1], Nikolay I. Ignatiev[1], Alexey Shakun[1], Andrey Patrakeev[1], Denis A. Belyaev[1], Jean-Loup Bertaux[1,3], Kevin S. Olsen[3], Lucio Baggio[3], Juan Alday[9], Yuriy S. Ivanov[5], Bojan Ristic[2], Jon Mason[6], Yannick Willame[2], Cédric Depiesse[2], Laszlo Hetey[2], Sophie Berkenbosch[2], Roland Clairquin[2], Claudio Queirolo[2], Bram Beeckman[2], Eddy Neefs[2], Manish R. Patel[6], Giancarlo Bellucci[7], Jose-Juan Lopez-Moreno[8], Colin F. Wilson[9], Giuseppe Etiope[7, 10], Lev Zelenyi[1], Håkan Svedhem[11], Jorge L. Vago[11] & the ACS and NOMAD Team*.

[1]Space Research Institute (IKI) RAS Moscow, Russia

[2]Royal Belgian Institute of Space Aeronomy BIRA-IASB, Brussels, Belgium

[3]LATMOS, UVSQ Université Paris-Saclay, Sorbonne Université, CNRS, France

[4]LMD CNRS Jussieu, Paris, France

[5]Main Astronomical Observatory MAO NASU, Kyiv, Ukraine

[6]Open University, Milton-Keynes, UK

[7]IAPS-INAF, Rome, Italy

[8]Instituto de Astrofìsica de Andalucía/CSIC, Granada, Spain

[9]Physics Department, Oxford University, Oxford, UK

[10]Istituto Nazionale di Geofisica e Vulcanologia, Rome, Italy; Faculty of Environmental Science and Engineering, Babes-Bolyai University, Cluj-Napoca, Romania.

[11]ESA-ESTEC, Noordwijk, the Netherlands

The detection of methane on Mars has been interpreted as indicating that geochemical or biotic activities could persist on Mars today[1]. A number of different measurements of methane show evidence for transient, locally elevated methane concentrations and seasonal variations in background methane concentrations[2-5]. These measurements, however, are difficult to reconcile with current understanding of the chemistry and physics of the Martian atmosphere[6, 7], which predicts the methane life time of several centuries resulting in its even, well mixed distribution[1, 6, 8]. Here we report highly sensitive attempts to detect atmospheric methane by the ACS and NOMAD instruments onboard the ESA-Roscosmos ExoMars Trace Gas Orbiter (TGO) from April to August 2018. We do not detect methane during the time period of our measurements and over a range of latitudes in both hemispheres. Our upper limit for methane of ~0.05 ppbv is 10-100 times lower than previously reported positive detections[2, 4]. We suggest that reconciliation between the present findings and the background methane concentrations found in Gale crater[4] would require an unknown process that can rapidly remove or sequester methane from the lower atmosphere before it spreads globally.

The first positive detections of methane on Mars were published in 2004 from the analysis of 1999 ground-based spectroscopic observations[9], and from the Planetary Fourier Spectrometer (PFS) instrument on board ESA's Mars Express orbiter[10]. Mixing ratios of methane of ~10 ppbv were reported. This stirred up excitement in the scientific community but both observations were at the limit of sensitivity. Another set of ground-based echelle-spectroscopy observations reported a plume of methane developed over 60 northern summer sols[2] in 2003, reaching a peak value of 45±10 ppbv. No or little methane (≤7–8 ppbv) was detected before and after this event[2, 11]. One more ground-based detection of 10 ppbv was reported in 2005[12]. Starting from October 2012 the Tunable Laser Spectrometer (TLS) of the Sample Analysis at Mars (SAM) instrument onboard NASA's Curiosity rover (MSL, Mars Science Laboratory) performed local samplings of Mars's atmosphere in Gale crater. The readings first remained below 2-3 ppbv, yet were followed by a number of positive detections in 2013-

2017, the most notable of 9 ppbv in January 2014[3]. This result was questioned in ref.[13] on the basis of potential rover self-contamination, an argument later rejected by the TLS team who showed such hypothesis was excluded based on a number of supporting evidences[4]. One of TLS detections of 5.8 ppbv in 2013[4] has been independently confirmed by PFS target observation of the Gale surroundings resulting in 15.5 ppbv value[5]. More sensitive TLS samplings led to the discovery of a seasonally varying "background level" ranging between 0.24 and 0.65 ppbv[4].

In the oxidizing martian atmosphere methane is slowly destroyed by UV photolysis and reactions with OH and O(^{1}D). Based on our current understanding of Mars photochemistry, it should have a lifetime of 250-300 years[1, 6, 8]. Therefore, its detection, even in small quantities, requires a sustained replenishment. Methane on Mars has attracted much interest because on Earth, most of the atmospheric methane has a biological origin. Thus the Martian atmospheric methane might hint at active or extant microbial life or at the existence of organic matter. However, methane can also be formed abiotically, by low-temperature chemical reactions (e.g., CO_2 hydrogenation) or magmatic processes[14, 15].

Given its potential implications for exobiology or geochemistry, highly sensitive measurements of atmospheric methane and other trace species were identified as the primary science goal of the TGO mission[16]. The 2-hour circular orbit of the TGO satellite was designed for detecting trace gases using solar occultations, a technique in which the spacecraft instruments observe the atmospheric absorption spectrum of sunlight during sunsets and sunrises[17]. Solar occultations provide very high sensitivity for trace gas concentration measurements because: (1) the Sun's brightness results in very high signal to noise ratio (SNR) spectra; and (2) the atmospheric optical path length in occultation viewing geometry is up to 10x longer than that achieved when observing the planet's surface. Two instrument suites on board TGO were designed to perform such measurements: ACS (the Atmospheric Chemistry Suite)[18] and NOMAD (Nadir and Occultation for MArs Discovery)[19]. Both ACS and NOMAD cover the 3.3 μm spectral range that includes the strongest fundamental absorption bands for hydrocarbons such as CH_4, in particular the ν_3 asymmetric stretching band on which all the

previous detections were made. TGO started its science operations in April 2018, with the first occultation taking place on April 21st. From June until August 2018 a planetary encircling dust storm has reduced the transparency of the atmosphere (see companion paper[20]), while high northern polar latitudes remained suitable for sensitive soundings. A map of measurements by the most sensitive channels of ACS and NOMAD in the CH_4 range is shown in Figure 1.

[Figure 1]

When staring at the solar disk outside the atmosphere, the SNR for ACS MIR (mid-IR) channel reaches 10,000 (one detector line, 2 s integration time, 2.5 km vertical sampling rate), and for NOMAD Solar Occultation (SO) channel SNR reaches ~2000 (one spectrum, 48 ms integration time, 1 km sampling rate). During a solar occultation, the trace gas detection sensitivity increases as the line of sight progressively samples closer to the surface, thereby intersecting a larger air mass. At the same time, sensitivity suffers from the increasing presence of dust and clouds, which can drastically reduce the intensity of light reaching the instrument. The atmospheric aerosol loading has previously been shown to have a negative effect on the retrieval accuracy at lower altitudes[18]. The optimum sensitivity is thus achieved at the lowest altitude where the atmosphere is still transparent enough, typically between 5 to 25 km corresponding to an atmospheric transmission of 0.2 to 0.5. Figure 2 shows examples of spectra acquired at an altitude close to the optimal one. No methane absorptions are apparent, while we accurately measure the faint H_2O lines within the range, which, at very low water content, have an absorption depth comparable to a 1 ppbv CH_4 absorption (panel c). Corresponding profiles of H_2O (see Methods), are characterized by an unprecedented accuracy compared to previous profiling[20, 21].

[Figure 2]

Based on the noise level, CH_4 absorption integrated over the line of sight can be tentatively fitted along with absorption of CO_2 while taking into account the instrument spectral resolution (see Methods). This way, an estimation of methane detection limits, converted into volume mixing ratios, for the full data set acquired by ACS and NOMAD was made. Figure 3 illustrates the detection limits

for the ensemble of observations performed by both instruments. The gradual increase in upper limits observed after the onset of the Planetary dust event (indicated by a light grey bar) is a direct consequence of dust forcing detections to occur progressively above 30 km, that is above the theoretically optimal altitude (detection-wise) usually found between 15 to 25 km. A few profiles, measured in cleaner northern conditions, were able to achieve the most precise detection limits of 0.012 ppbv down to an altitude of ~3 km (cf. Figure 3).

[Figure 3]

This non-detection of methane by TGO and its associated upper limits are in contradiction with the 0.41 ppbv background levels measured *in situ* by Curiosity at the same season[4] in previous years. As discussed above, TGO is able to detect concentrations at least ten times lower than 0.4 ppbv. In fact, a simple comparison of the theoretical sensitivity of the solar occultation method with the TLS instrument method shows that TGO should be more sensitive than what can be achieved with the TLS, even when the measurements are performed using the TLS enrichment mode (see Methods).

Is it possible that the factor of ten difference between the MSL measurements and the TGO upper limits could result from spatial variations in the methane mixing ratios? MSL measurements were obtained at the bottom of Gale Crater near the equator, while the best TGO measurements were achieved in the near-polar latitudes and a few kilometres above the surface. However, It is difficult to understand why the Martian atmosphere would permit such a spatial differentiation of concentrations. On Mars, the daytime atmospheric boundary layer is characterized by intense convective motions, which mix any trace gas such as methane efficiently on a daily basis from the surface up to the top of the convective boundary layer, usually 6 to 10 kilometres high. From there the global wind circulation transports trace gases horizontally[6, 22] and vertically around the planet. Global uniform mixing of methane occurs on a scale of 2 to 3 months[6, 8, 23]. Even in the extremely unlikely case where Gale Crater would constitute the sole source of methane on Mars (note that Gale Crater and surrounding areas along the Martian dichotomy host geological features where methane could be released[13]), MSL measurements still remain in disagreement with the detection limits derived

from TGO measurements. Indeed, considering only the background concentration of 0.41 ppbv we assume that Gale is uniformly and constantly filled with CH_4 up to its lowest rim (at ~2 km) and that a mixing timescale of 1 sol^{-1} (ref.[4]) is the typical time for air to leave the crater. The Gale emission would lead CH_4 to accumulate globally over one Martian year at a level of ~2 pptv. This implies that such a background emission from Gale crater could only have been going on for at most 24 Martian years (or 44 Earth years) before the detection limits reported here would have been reached. Taking into account the ppbv spikes of CH_4 concentration reported by MSL, this 24 years timeframe would be even more shortened. This is unrealistic. To maintain a level of methane ten times higher than elsewhere, Gale Crater should not only be the unique source, it should also preserve its air mass from exchanging with the global atmosphere. Interestingly, mesoscale model simulations have shown that the depth of the boundary layer in Gale crater is significantly lowered[24] due to the crater size and depth. Even if this would tend to maintain methane locally, the same simulation [24, 25] shows that the slope winds on the side of the crater and the induced updraft above the rims is so intense that methane should be efficiently injected into the atmosphere at 10 km altitude. In no case can we consider Gale to be an isolated crater (see Methods for additional information).

To reconcile the lack of CH_4 detection in the TGO data and the positive CH_4 detection at the surface by Curiosity, one must invoke a mechanism able to fully eradicate methane in the lower atmosphere at a rate ~1000 times faster than that predicted by the conventional chemistry. However, existing conventional models not only describe very well the chemistry of methane on Earth but also reproduce satisfactorily on Mars species that are sensitive to the oxidizing capacity of the atmosphere, such as hydrogen peroxide[26], ozone[27], and carbon monoxide[28]. Unless a mechanism is discovered that can rapidly destroy or sequester methane and is compatible with our wide quantitative understanding of Mars photochemistry, all the methane detections reported to date appear inconsistent with present TGO measurements.

References

1. Yung, Y. L. et al. Methane on Mars and Habitability: Challenges and Responses. Astrobiology, doi:10.1089/ast.2018.1917 (2018).
2. Mumma, M. J. et al. Strong Release of Methane on Mars in Northern Summer 2003. Science 323,1041-1045, doi:10.1126/science.1165243 (2009).
3. Webster, C. R. et al. Mars methane detection and variability at Gale crater. Science 347,415-417 (2015).
4. Webster, C. R. et al. Background levels of methane in Mars' atmosphere show strong seasonal variations. Science 360,1093-1096 (2018).
5. Giuranna, M. et al. Independent confirmation of a methane spike on Mars and a source region east of Gale Crater. Nature Geoscience, accepted (2019).
6. Lefèvre, F. & Forget, F. Observed variations of methane on Mars unexplained by known atmospheric chemistry and physics. Nature 460,720-723 (2009).
7. Zahnle, K., Freedman, R. S. & Catling, D. C. Is there methane on Mars? Icarus 212, 493-503, doi:10.1016/j.icarus.2010.11.027 (2011).
8. Viscardy, S., Daerden, F. & Neary, L. Formation of layers of methane in the atmosphere of Mars after surface release. Geophysical Research Letters 43, 1868-1875 (2016).
9. Krasnopolsky, V. A., Maillard, J. P. & Owen, T. C. Detection of methane in the Martian atmosphere: evidence for life? Icarus 172,537-547 (2004).
10. Formisano, V., Atreya, S., Encrenaz, T., Ignatiev, N. & Giuranna, M. Detection of Methane in the Atmosphere of Mars. Science 306,1758-1761 (2004).
11. Villanueva, G. L. et al. A sensitive search for organics (CH4, CH3OH, H2CO, C2H6, C2H2, C2H4), hydroperoxyl (HO2), nitrogen compounds (N2O, NH3, HCN) and chlorine species (HCl, CH3Cl) on Mars using ground-based high-resolution infrared spectroscopy. Icarus 223,11-27 (2013).

12. Krasnopolsky, V. Search for methane and upper limits to ethane and SO2 on Mars. Icarus 217,144-152, doi:10.1016/j.icarus.2011.10.019 (2012).
13. Zahnle, K., 2015. Play it again, SAM. Science 347, 370–371. https://doi.org/10.1126/science.aaa3687
14. Etiope, G. & Sherwood Lollar, B. Abiotic Methane on Earth. Reviews of Geophysics 51, 276-299 (2013).
15. Oehler D. & Etiope G. Methane seepage on Mars: where to look and why. Astrobiology 17, 1233-1264 (2017).
16. Vago, J. et al. ESA ExoMars program: The next step in exploring Mars. Solar System Research 49,518-528 (2015).
17. Svedhem, H., Vago, J. L., Mitschdörfer, P., de Groot, R., Montagna, M., Renaud, P.-Y. The ExoMars Trace Gas Orbiter, Space Sci. Rev. 215. In press (2019).
18. Korablev, O. et al. The Atmospheric Chemistry Suite (ACS) of three spectrometers for the ExoMars 2016 Trace Gas Orbiter. Space Sci. Rev. 214:7, doi:10.1007/s11214-11017-10437-11216 (2018).
19. Vandaele, A. C. et al. NOMAD, an integrated suite of three spectrometers for the ExoMars Trace Gas mission: technical description, science objectives and expected performance. Space Sci. Rev. 214:80, doi:10.1007/s11214-018-0517-2 (2018).
20. Vandaele, A. C. et al. Martian dust storm impact on atmospheric water vapour observed by ExoMars Trace Gas Orbiter. Nature, in press (this issue 2019).
21. Fedorova, A. et al. Water vapor in the middle atmosphere of Mars during the 2007 global dust storm. Icarus 300, 440-457, doi:10.1016/j.icarus.2017.09.025 (2018).

22. Mischna, M. A., Allen, M., Richardson, M. I., Newman, C. E. & Toigo, A. D. Atmospheric modeling of Mars methane surface releases. Planetary and Space Science 59, 227-237, doi:10.1016/j.pss.2010.07.005 (2011).
23. Waugh, D. W., Toigo, A. D. & Guzewich, S. D. Age of martian air: Time scales for martian atmospheric transport. Icarus 317, 148-157, doi:10.1016/j.icarus.2018.08.002 (2019).
24. Tyler, D. & Barnes, J. R. Convergent crater circulations on Mars: Influence on the surface pressure cycle and the depth of the convective boundary layer. Geophysical Research Letters 42,7343-7350 (2015).
25. Vasavada, A. R. et al. Assessment of Environments for Mars Science Laboratory Entry, Descent, and Surface Operations. Space Science Reviews 170, 793-835 (2012).
26. Clancy, R. T., Sandor, B. J. & Moriarty-Schieven, G. H. A measurement of the 362 GHz absorption line of Mars atmospheric H2O2. *Icarus* **168**, 116-121 (2004).
27. Clancy, R. T. et al.. (2016). Daily global mapping of Mars ozone column abundances with MARCI UV band imaging. Icarus 266, 112–133. https://doi.org/10.1016/j.icarus.2015.11.016(2016).
28. Smith, M.D. et al. The climatology of carbon monoxide and water vapor on Mars as observed by CRISM and modeled by the GEM-Mars general circulation model. Icarus 301,117–131. https://doi.org/10.1016/j.icarus.2017.09.027(2018).

Figure captions

Figure 1. Map of ExoMars TGO methane measurements by ACS (stars) and NOMAD (circles) used in this study. The symbols, corresponding to example measurements considered in this study are enlarged. The colour scale denotes L_s (the areocentric Solar Longitude). Gale crater (the Curiosity rover location) is marked by a bold, black square.

Figure 2. TGO spectra encompassing the spectral range with multiple methane R-branch features. Panels **a, b**: Example of spectra obtained by NOMAD SO in two different ranges. The measurements are plotted together with synthetic models of CH_4 and of water vapour absorption. Panel **c**: similar results obtained by ACS MIR before the dust storm. The ACS spectrum includes the same methane feature of methane as in Panel **b** (3048.2 cm^{-1}), and two stronger isolated features, allowing to constrain the methane content below few tens of pptv. Measured spectra show 1-σ instrument noise. The tangent altitudes above areoid are indicated.

Figure 3. Upper limits for CH_4 (95% confidence limit) obtained by TGO (ACS and NOMAD) compared to seasonally variable background methane as measured by SAM-TLS on Curiosity. The colour scale gives the latitude of the TGO sampling. The TGO dataset has been filtered to retain only the most precise upper limits below a threshold of 0.15 ppbv, encompassing values down to 0.012 ppbv. The gradual increase in upper limits is associated with the onset of the Planetary dust event (indicated by a light grey bar.

Acknowledgements

ExoMars is the space mission of ESA and Roscosmos. The ACS experiment is led by IKI, Space Research Institute in Moscow, assisted by LATMOS in France. The project acknowledges funding by Roscosmos and CNES. Science operations of ACS are funded by Roscosmos and ESA. IKI affiliates acknowledge funding under grant #14.W03.31.0017 and contract #0120.0 602993 (0028-2014-0004) of Russian Government. The NOMAD experiment is led by the Royal Belgian Institute for Space Aeronomy (IASB-BIRA), assisted by Co-PI teams from Spain (IAA-CSIC), Italy (INAF-IAPS), and the United Kingdom (Open University). This project acknowledges funding by the Belgian Science Policy Office (BELSPO), with the financial and contractual coordination by the ESA Prodex Office (PEA 4000103401, 4000121493), by Spanish MICINN through its Plan Nacional and by European funds under grants ESP2015-65064-C2-1-P and ESP2017-87143-R (MINECO/FEDER), as well as by UK Space Agency through grants ST/R005761/1, ST/P001262/1, ST/R001405/1, ST/S00145X/1, ST/R001367/1, ST/P001572/1 and ST/R001502/1, and Italian Space Agency through grant 2018-2-HH.0. This work was supported by the

Belgian Fonds de la Recherche Scientifique - FNRS under Grant n°30442502 (ET_HOME). We are indebted to the large number of people responsible for designing, building, testing, launching, communicating to, operating the spacecraft and science instruments, whose efforts made the success of TGO possible.

Author contributions

O.K., A.C.V., F.M. conceived the study, collected inputs and wrote the paper. A.A.F. calibrated the ACS data and analysed the profiles assisted with A.T., K.S.O., J.A. The ACS dataset was prepared by A.T. assisted by L.B., J.A.P., and Y.S.I. A.T, A.G., N.I., A.S., and A.P. have designed ACS observations. D.B. analysed ACS CO_2 data. F.M. has derived the methane detection limits from ACS. I.R.T. analysed the solar occultation data and provided transmittances from NOMAD SO. J.T.E. and L.T. with S.A. derived the NOMAD methane detection limits. J.T.E. and S.R. provided and analysed the a priori knowledge and initial GCM fields, the latter were provided by L.N. and F.D. C.D. and Y.W. were involved in UVIS calibration and data pipeline. B.R., B.B., C.Q., and E.N. designed the NOMAD observations helped by J.M. for the UVIS channel. L.H., S.B., and R.C. are responsible for the uplink and downlink of telemetry and science data, and first conversion of those to scientific data. M.R.P., G.B. and J.J.L.M. provided support in the selection of the NOMAD observations based on scientific interest. F.F., F.L., F.D., provided critical inputs regarding the model chemistry and circulation, assisted with J.L.B., L.N., S.V., and G.E. C.W., L.Z. and H.S. coordinated observations of the various instruments on TGO. All authors contributed to the preparation of the manuscript.

The authors declare no competing interests.

***The ACS and NOMAD Team** Gustavo Alonso-Rodrigo[12], Francesca Altieri[7], Konstantin Anufreychik[1], Gabriele Arnold[13], Sophie Bauduin[14], David Bolsee[2], Giacomo Carrozzo[7], R. Todd Clancy[15], Edward Cloutis[16], Matteo Crismani[17], Fabiana Da Pieve[2], Emiliano D'Aversa[7], Natalia Duxbury[18], Therese Encrenaz[19], Thierry Fouchet[19], Bernd Funke[8], Didier Fussen[2], Maia Garcia-Comas[8], Jean-Claude Gérard[20], Marco Giuranna[7], Leo Gkouvelis[20], Francisco Gonzalez-Galindo[8], Davide Grassi[7], Sandrine Guerlet[4], Paul Hartogh[21], James Holmes[6], Benoît Hubert[20], Jacek Kaminski[22], Ozgur Karatekin[23], David

Kass[24], Yasumasa Kasaba[25], Igor Khatuntsev[1], Armin Kleinbohl[24], Nikita Kokonkov[1], Vladimir Krasnopolsky[26, 27], Ruslan Kuzmin[28, 1], Gaétan Lacombe[3], Orietta Lanciano[29], Emmanuel Lellouch[19], Stephen Lewis[6], Mikhael Luginin[1], Giuliano Liuzzi[17], Manuel López-Puertas[8], Miguel Lopez-Valverde8, Anni Määttänen[3], Arnaud Mahieux[2], Emmanuel Marcq[3], Javier Martin-Torres[30,31], Igor Maslov[1], Alexander Medvedev[21], Boris Moshkin[1], Michael Mumma[17], Hiromu Nakagawa[25], R. Novak[17], Fabrizio Oliva[7], Dimitry Patsaev[1], Arianna Piccialli[2], Etienne Renotte[32], Birgit Ritter[20], Alexander Rodin[27], Frédéric Schmidt[33], Valery Shematovich[34], Michael Smith[17], Nick Teanby[35], Ed Thiemann[36], Nicolas Thomas[37], Jean Auwera Vander[14], Luis Vazquez[38], Geronimo Villanueva[39], Matthieu Vincendon[40], Jim Whiteway[41], Valérie Wilquet[2], Michael Wolff[15], Paulina Wolkenberg[7], Roger Yelle[42], Ludmila Zasova[1] & Maria Paz Zorzano[30,43].

Affiliations for participants: [12]IDR-UPM, Madrid, Spain. [13]DLR, Institute of Planetary Research, Berlin, Germany. [14]Université Libre de Bruxelles, Belgium.[15]Space Science Institute, USA. [16]University of Winnipeg, Canada. [17] NASA GSFC, USA. [18] Moscow University, Russia; [19] LESIA, Observatoire de Paris Meudon, France; [20]Université de Liège, Belgium; [21]Max Planck Institute, Göttingen, Germany. [22]Institute of Geophysics PAS, Warszawa, Poland. [23] Royal Observatory, Brussels, Belgium. [24]NASA JPL, USA. [25] Tohoku University, Sendai, Japan. [26] Catholic University of America, Washington, DC USA. [27]MIPT, Dolgoprudnyi, Moscow reg., Russia. [28] Vernadsky Institute RAS, Moscow, Russia. [29]ASI Italy. [30]Luleå University of Technology, Sweden.[31] CSIC-UGR, Granada, Spain. [32]ATMOS, Belgium. [33]GEOPS/Univ Paris Sud, France. [34]Institute of Astronomy RAS, Moscow, Russia. [35]University of Bristol, UK. [36]LASP, Boulder CO, USA. [37]University of Bern, Switzerland. [38]Universidad Complutense de Madrid, Spain. [39]CUA USA. [40]IAS, Université Paris Sud, Orsay, France. [41]York University, Canada. [42]LPL Tucson AZ USA. [43]INTA-CSIC, Madrid, Spain.

Methods

ACS instrument and measurements

ACS[18] consists of three infrared channels featuring high accuracy, a high resolving power, and broad spectral coverage (0.7 to 17 μm). The mid-infrared (MIR) channel is a high dispersion echelle spectrometer dedicated to solar occultation measurements in the 2.3-4.5 μm range. MIR has been conceived to accomplish the most sensitive measurements of Martian trace gases, while simultaneously profiling more abundant compounds such as CO_2, H_2O, and their isotopologues. ACS MIR is a crossed dispersion spectrometer which measures spectra dispersed onto a cryogenic 512×640 CdHgTe infrared array. For each acquired frame, MIR measures ≥20 adjacent diffraction orders, covering an instantaneous spectral range of 0.15 to 0.3 μm wide. To achieve the full spectral coverage, a secondary dispersion grating can be rotated to one out of 12 distinct positions (see[17] for a tabulated description of all the grating positions). Together with two other channels, the near-infrared (NIR) and the thermal infrared Fourier transform (TIRVIM) spectrometers, ACS continuously covers the spectral range between 0.7 and 17 μm. NIR and TIRVIM channels are used to observe, both in solar occultation and in nadir, water vapour H_2O, carbon monoxide CO, and other gases including molecular oxygen O_2 in a fundamental state. The broad spectral range acquired enables the characterization of the key meteorological parameters, including dust and water ice cloud column opacities. In addition, the temperature profile of the atmosphere can be retrieved from the 15-μm CO_2 band sensed by TIRVIM in nadir.

In this work, we used ACS MIR data obtained with the secondary grating tuned to position #12. In this range, MIR acquires frames containing 20 adjacent and partially overlapping diffraction orders (from #172 to #192) from 3.09 μm to 3.45 μm (Figure 4). The instrument point-spread-function (PSF) can be assimilated to a Gaussian function associated with a spectral resolving power of $\lambda/\Delta\lambda>30{,}000$ where $\Delta\lambda$ is taken as the full-width at half-maximum (FWHM) of the Gaussian, that is $\sim 2.36 \times \sigma$ (with σ, the standard deviation). ACS MIR was operated in the so-called "high-sensitivity" mode, where 200 frames obtained from consecutive 6 ms integration frames are stacked together on-board. One full measurement lasts 2.1 seconds. Depending on orbital parameters a profile of the atmosphere from 0 to 200 km is measured within 3 to 6 minutes. The uppermost part of the

occultation corresponds to the clear sun observations, averaged to obtain a reference spectrum $\boldsymbol{I}_{sun}$. A dark signal $\boldsymbol{I}_{dark}$ (the sum of detector dark current and of the surrounding thermal background emission) is estimated from the dark part of the occultation where the sun is fully obscured by the solid body of Mars and is refined using dedicated observations of the open space. As the thermal environment inside the instrument is slightly changing during the occultation session due to internal and solar heating, $\boldsymbol{I}_{sun}$ and $\boldsymbol{I}_{dark}$ are also time-dependent. To account for the gradual sub-pixel drift of the image during the occultation, we extrapolate the trend of each pixel measured during the clear sun observation throughout the occultation. The methane spectral range around 3030 cm^{-1} is free of any strong gaseous absorptions, and the atmosphere above 100 km can be considered clear from any absorptions features, increasing the accuracy of the extrapolation. Each line of the detector within each stripe represents a transmittance spectrum at a certain altitude and at a wavelength range corresponding to the displayed diffraction. The resulting frame of transmittances undergoes a projective transformation to correct the artefactual curved appearance of the stripes of each diffraction order and to make it look more horizontal and thereby maintain spectral connectivity between adjacent orders (see Extended Data Figure 1). A first-order approximation of the pixel-to-wavelength calibration is established using solar lines and is then refined using the strong absorption lines of CO_2 or H_2O.

NOMAD instrument and measurements

NOMAD[19] includes three spectroscopic channels, operating from the ultraviolet (UV) and visible range to 4.3 µm. The channel most sensitive to trace gases is the SO (Solar Occultation) spectrometer providing a spectral resolving power of $\lambda/\Delta\lambda \approx 20{,}000$ in the spectral range of 2.3-4.3 µm. Within this range, NOMAD SO acquires 10 separate wavelength sub-ranges to profile a variety of atmospheric species. The two other channels of NOMAD are the UVIS (Ultraviolet and visible spectrometer; 200-650 nm), and LNO (Limb, Nadir, Occultation) spectrometers that can be operated both in solar occultation and in nadir. NOMAD provides vertical profiling information for atmospheric constituents at unprecedented spatial and temporal resolution. Indeed, in solar occultation, the

vertical resolution is less than 1 km for SO and UVIS, with a sampling rate of 1 s (one measurement every 1 km), and occultations range from the surface to 200 km altitude. NOMAD also provides mapping of several constituents (aerosols/dust/clouds, and O_3, H_2O, HDO, CO, and other trace gases) in nadir mode with an instantaneous footprint of 0.5 x 17 km^2 (LNO spectrometer) and 5 km^2 (UVIS spectrometer) respectively, with a repetition rate of 30 Martian days.

For this work, we analysed SO channel data measured between 21 April and 1 August. SO measures 4 spectral bins in each of 5 or 6 diffraction orders per second in solar occultation mode, among which a series of specific diffraction orders were chosen (order 133 to 136 spanning 2990 to 3080 cm^{-1} spectral range) where methane features are located. To increase the sensitivity of the NOMAD SO measurements, we accumulate all the spectral measurements in each occultation from the 4 detector bins into 3 km vertical bins. The transmittance calibration and error calculation as described by Trompet et al.[29] is adapted to consider this accumulation. By accumulating multiple measurements we improve the SNR, by increasing the 48 ms integration time for a single detector bin to an effective integration time of 144 ms for all illuminated detector bins. By accumulating multiple measurements, we effectively increase the typical 48 ms integration time of a single measurement to an average of 500 ms integration, thereby increasing the SNR as compared to the previous estimation[30].

Calculation of the methane detection limits

Attempting to detect methane we have used the ACS data from diffraction orders #180 (which contains the Q-branch of the fundamental ν_3 asymmetric stretching band of CH_4), and #182 (which contains the strongest lines among the P- and R-branches) as shown in Extended Data Figure 1, and described in the main text. Five detector lines were stacked together to form a spectrum to be fitted. We then applied a method to retrieve vertical profiles of trace gas vmr as developed for Mars Express solar occultaton[21, 31]. First, a more accurate wavelength-to-pixel dependence is established using the most intense H_2O absorption lines and is then propagated elsewhere in the occultation in particular where the water lines are too faint. Finally, the vmr profiles of the trace constituents are retrieved by

fitting the retrieved occultation portion with a pre-computed look-up synthetic model in a three-parameter space (H_2O, CH_4 vmr, and aerosol extinction) using Rodgers' regression with additional Tikhonov regularization[32]. The synthetic spectra were computed with spectral line parameters from HITRAN 2016[33] corrected to account for the CO_2 atmosphere, as described in[21]. Temperature and pressure profiles were extracted from the Mars Climate Database[34]. Aerosol extinction is assumed to have a grey behaviour within a diffraction order. The retrieved profiles of H_2O and the attempts to retrieve CH_4 for two selected occultations are shown in Extended Data Figure 2. The H_2O profiles, even though obtained from faint lines corresponding to very dry conditions, are nevertheless characterized by a greater accuracy compared to previous H_2O profilings[21]. However, this formal retrieval shows no trace of methane. Sometimes very small methane abundances of ~20 pptv in the R-branch (3058 cm^{-1}) were retrieved above the 1-σ level. However, this result was not confirmed, in any case, by a corresponding result in the Q-branch (3018 cm^{-1}). We conclude that these constitute false positive detections, perhaps due to a residual fixed pattern noise in the spectrum. The effect of the atmospheric aerosol loading on the retrieval accuracy is illustrated in the right panel where the "profile" of transmittance noise is shown along with the optical slant density, as measured along the line of sight.

As no methane was detected within the analysed dataset, we selected a faster approach to estimate robust upper limits of CH_4vmr for the considered dataset covering the April to August period of 2018. The sensitivity in solar occultation is produced by the number of species molecules observed along the LOS. We assume that no methane can be retrieved within the 1-σ error bars.

Near the centre of the detector, the best SNR are achieved at a level of ≥10,000. This very low noise level implies that the main source of errors is systematic. This is the fixed pattern noise. The part of the systematic error originating from the detector dark current non-uniformity (DCNU) is not fully cancelled out when divided by solar reference $\boldsymbol{I}_{sun}$ because of the non-linearity of the detector pixels. This noise appears as a pattern with a relative level of $\leq 10^{-3}$ exhibiting a pixel-to-pixel correlation remanent on consecutive spectra. In Figure 2, the fixed pattern noise is responsible for

most of the visible irregularities, while the random noise (error bars shown by hairlines) only becomes visible near the edges of the detector where the signal is weaker.

To account for both the fixed pattern and the random noise, we define the instrument noise as the standard deviation of a transmission spectrum filtered from all pixel correlation wider than 2 pixels and computed over most of the diffraction order. This calculation overestimates noise in case of spectrally narrow gaseous absorptions (since the broader ones are filtered) whose signature leaks in the pixel-to-pixel variation. We inferred directly the line-of-sight (LOS) density, which is the number of molecules integrated along the line of sight N [cm^{-2}] of putative methane with that of CO_2, simultaneously measured in diffraction order #178. CH_4 LOS density is estimated separately using either the CH_4 Q-branch in order #180 (3015-3022 cm^{-1}) or the deepest R-branch feature that can be found in order 182 (3057-3060 cm^{-1}), see Figure 2.

By considering that CH_4 can be loosely detected if the tentatively retrieved value exceeds its error bar, an upper limit on CH_4 is deduced separately for the Q and R branches by assuming it to be equivalent to the error bar found for the CH_4 LOS density. A multivariate regression algorithm based on a Levenberg-Marquardt approach (MPFIT.pro IDL routine of C. Markwardt based on MINPACK-1) was used for all retrieval attempts. This algorithm provides as an output the covariance matrix of the fitted parameters whose diagonal values correspond to the square of the error bar of every parameter. The upper limit on CH_4 vmr is then defined as the retrieved error of the CH_4 LOS density divided by the CO_2 LOS density. The uncertainty on CO_2 is ignored, as it accounts for only a minor fraction of the upper limit. A correspondence between the instrument SNR and the CH_4 LOS density detection limit can be theoretically established. The detection limit, and the step-by-step outputs of the retrieval are shown in Extended Data Figure 3 , with the resulting upper limits vs. altitude in Extended Data Figure 4.

A similar simplified retrieval method was used to estimate the detection limit from NOMAD spectra. The forward model computes the optical column density for each spectrum separately, assuming a constant mixing ratio along the line-of-sight and using the most recent HITRAN[33] CH_4 line

list with CO_2 pressure broadening coefficients. The optical depth is then convoluted to the instrument's PSF with FWHM of 0.15 cm^{-1} and then multiplied by the grating blaze and AOTF functions. The transmittance spectra are fit by minimizing the chi-squared using the Levenberg-Marquardt algorithm (via the Python Scipy wrapper of MINPACKS *lmder*[35]) to determine an optimal polynomial background and CH_4 mixing ratio. The standard error of the mixing ratio is derived from the covariance matrix of the optimal fit parameters. This value can be thought of as the symmetric error bound on the mixing ratio that can affect the transmittance within the measurement noise and should be a close approximation to the detection limit.

Comparing the sensitivity of TGO solar occultations to that of SAM TLS.

The SAM laser spectrometer onboard Curiosity measures gaseous absorption using an atmospheric sample in a 16.2 meters path length cell at ambient Mars pressure (~8 mbar)[36]. The number of air (CO_2) molecules interacting with the laser beam (the column density) is $N \approx 2 \cdot 10^{20}$ cm^{-2}. Very high spectral resolution of TLS allows for resolving the natural, pressure-broadened linewidth of two methane absorption lines of ~$10^{-2}$$cm^{-1}$. For a subset of samplings, TLS was operated in a more sensitive mode where CO_2, which constitutes 96% of the atmosphere, was progressively removed from the sample enriching the remaining gases by a factor of 20-25. The achieved accuracy is 1-2 ppbv of methane for the direct intake, and 50-100 pptv for the enrichment mode[3, 4, 36].

For solar occultation geometry, the number of CO_2 molecules along the line of sight at a slant altitude of 20 km is $N \approx 10^{24}$ cm^{-2}, increasing as sounding closer to the surface (see Figure 6). The spectral resolution, as confirmed in flight, is ~0.1 cm^{-1} for the ACS MIR channel, and ~0.15 cm^{-1} for NOMAD SO. ACS and NOMAD spectra give access to multiple strong features of methane around the 3.3 μm range. Neglecting other factors, such as noise, systematic errors, contamination, etc. potentially affecting both methods, one can estimate that the TGO occultation measurements are theoretically a factor of ≥1000x more sensitive than what can be achieved with the TLS direct intakes, and of ≥30x more sensitive comparing to measurements performed in the enrichment mode.

Can we reconcile TGO and MSL measurements?

The mass of CH_4 in Gale crater if filled to the lowest rim can be calculated as follows: The Gale crater diameter is 154 km and its lowest rim is 2 km high, resulting in $6.7 \cdot 10^{11}$ kg of air or $9.3 \cdot 10^{36}$ molecules. The amount of CH_4 corresponding to 0.41 ppbv content is $0.41 \cdot 9.3 \cdot 10^{27}$ molecules or 100kg of CH_4. More accurately, using MOLA topography and GCM atmospheric profiles we find 30 kg of CH_4, as Gale is not a perfect cylinder and the air density decreases with height.

There is no reason to consider the 10 random measurements by SAM's TLS of 0.41 ppbv on average in a two year period[4] to coincide with transient methane releases, so we assume that amount is present at all days during the martian year. Ref.[4] estimated the mixing rate to be 1 sol^{-1}, meaning that the methane in the crater is replenished every sol. So the total mass of CH_4 emitted in Gale crater over one martian year is 20 tons or $7.5 \cdot 10^{29}$ molecules. The full mass of the atmospheres is $2.6 \cdot 10^{16}$ kg, giving $2 \cdot 10^{-12}$ or 2 pptv of CH_4 well mixed. In 24 martian years (or 44 Earth years) this accumulates to 50 pptv, and this just with a single source in Gale. Transient enrichments of methane, observed remotely[2], and spikes detected by SAM's TLS[3] further accelerate the accumulation rate.

To make the TGO and TLS-SAM results consistent (i.e. an accumulation of 50 pptv over 300 years), the mixing inside/outside Gale would have to be lower than 1 sol^{-1} by a factor of ~7. This large factor is in full contradiction with mesoscale simulations, and with the strong slope winds[24, 25]. A newer simulation[37] also shows that one should not expect Gale Crater to trap any trace gas for longer than 1 sol. They were looking at water vapour, which was largely released by sublimation of overnight surface ice, and was then mixed up above 3 km (compared to MOLA, so already several km above the crater's highest rim) by noon and very well mixed by 4pm on the same day. A trace gas mixed over this height range is then rapidly transported out of Gale Crater by the afternoon upslope winds, combined with the lower branch of the Hadley Circulation (northward or southward, depending on time of year). The majority of any release at 6am had left the crater by 6am on the next day.

Finally, the dust event 2018A affecting a subset of our measurements could not substantially bias the conclusions of present study. First, we establish stringent upper limits on methane before the event, and during the event in the polar areas. Second, the fact that the H_2O_2 measured in dusty

conditions is well reproduced by conventional models (despite the strong sensitivity of that species to the oxidizing capacity of the atmosphere) does not suggest the existence of any major chemical mechanism on mineral dust[26, 38].

29. Trompet, L. *et al.* Improved algorithm for the transmittance estimation of spectra obtained with SOIR/Venus Express. *Applied Optics* **55**, 9275-9281, http://dx.doi.org/10.1364/AO.55.009275 (2016).
30. Liuzzi, G. *et al.* Methane on Mars: New insights into the sensitivity of CH4 with the NOMAD/ExoMars spectrometer through its first in-flight calibration. *Icarus* **321**, 671-690, doi:10.1016/j.icarus.2018.09.021 (2019).
31. Maltagliati, L. *et al.* Annual survey of water vapor vertical distribution and water–aerosol coupling in the Martian atmosphere observed by SPICAM/MEx solar occultations. *Icarus* **223**, 942-962 (2013).
32. Rodgers, C. D. Inverse Methods for Atmospheric Sounding. Vol. 2 (World Scientific, 2000).
33. Gordon, I. E. *et al.* The HITRAN2016 Molecular Spectroscopic Database. *J. Quant. Spectrosc. Radiat. Transfer* **203**, 3-69, doi:10.1016/j.jqsrt.2017.06.038 (2017).
34. Millour, E.*et al.* The Mars Climate Database (MCD version 5.2). *European Planetary Science Congress 2015, held 27 September - 2 October, 2015 in Nantes, France, Online at http://meetingorganizer.copernicus.org/EPSC2015</A>, id. EPSC2015-43810* (2015).
35. More, J., Garbow, B., Hillstrom, K. User Guide for MINPACK-1. Technical Report ANL-80-74, Argonne National Laboratory (1980).
36. Webster, C. R. et al. Low Upper Limit to Methane Abundance on Mars. *Science* **342,** 355-357 (2013).

37. Steele, L. J., Balme, M. R., Lewis, S. R. & Spiga, A. The water cycle and regolith-atmosphere interaction at Gale crater, Mars. *Icarus* **289**, 56-79 (2017).

38. Lefèvre, F. & Krasnopolsky, V. Atmospheric Photochemistry. In *The atmosphere and climate of Mars - ACM2017* (ed. Robert M. Haberle) 374-404 (Cambridge University Press 2017).

Data availability

The datasets generated by the NOMAD and ACS instruments and analysed during the current study will be available in the ESA PSA repository, https://archives.esac.esa.int/psa, after the six-months prior access period following ESA Rules on Information, Data and Intellectual Property. The data used for the figures are available on request from the corresponding author O.K.

Code availability

The computer codes used to decipher the upper limits of CH_4 are available on request from the corresponding author O.K.

Extended data figure captions

Extended Data Figure 1. A sequence of transmittance spectra measured with ACS MIR channel for an example orbit (Ls=180.9°) obtained using the secondary grating position #12[17]. Different diffraction orders are denoted by changing colour of the transmission curves, and their numbers are indicated at the upper scale. Diffraction orders used in this study are #178 (for CO_2), #180 (CH_4 QR-branch), and #182 (CH_4 RQ-branch). Enhanced extinction on the short wavelength edge of the spectra is due to H_2O ice absorption.

Extended Data Figure 2. Retrieval of trace gases from ACS MIR spectra using Rodger's regression illustrated for one aerosol-free polar case (upper panels), and for a more cloudy low-latitude case (lower panels). Both occultations were observed before the global dust event. Left panels: water vapour profiles retrieved using faint H_2O absorption lines separately in diffraction orders #180 and #182. Middle panels: attempts to retrieve CH_4 in the same diffraction orders. Curves with error bars indicate the regularized profiles. The error bars give the 1-σ uncertainty on the retrieved

parameters. To illustrate the accuracy for the individual spectra, the regularization was also turned off (scatter points). Right panels: profiles of the optical depth on the line of sight, and of the signal-to-noise ratio (SNR) in the MIR spectra. The SNR for each spectrum was calculated over the whole diffraction order, excluding spectral intervals with gaseous features.

Extended Data Figure 3. Top: the theoretical relation between SNR/pixel and the retrieved 1-σ uncertainty on the CH_4 line-of-sight density expressed in molecules·cm^{-2}. At SNR > 1,000/pixel, the associated uncertainty is 10^{14} molecules·cm^{-2}, which would yield an equivalent vmr uncertainty of 0.1 ppbv of CH_4 in the 10 km altitude range where the CO_2 density is usually around 10^{24} molecules·cm^{-2}. Bottom, from left to the right: Altitude profiles of (left) SNR / pixel, (middle) CO_2 and error on CH_4 LOS density in cm^{-2}, and (right) resulting upper limits retrieved for CH_4 molecules. The displayed observation corresponds to high northern latitudes after equinox (Ls 192°). The prevailing clear conditions allowed sounding very close to the surface with high SNR, yielding optimal conditions for the retrieval of CH_4. The black, red and blue colours refer respectively to CO_2, (in order #178), CH_4 (in order #180) and CH_4 (in order #182).

Extended Data Figure 4. A compilation of all the retrieved upper limits from the ACS-MIR dataset covering the period from April 21st to September 4th 2018 using (Top) the Q-branch, and (bottom) the R-branch of CH_4 absorption. The colour scale denotes L_s. Symbols of alike colour denote individual profiles.

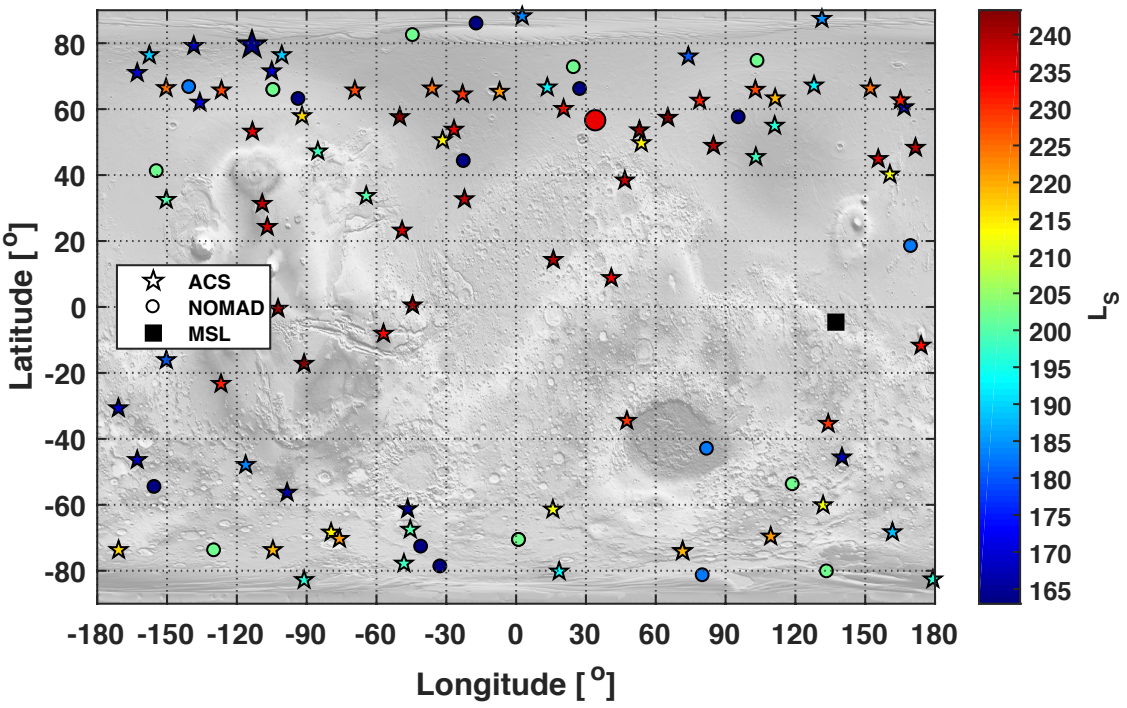
ACS
NOMAD
MSL
Latitude [°]
80
60
40
20
0
-20
-40
-60
-80
-180 -150 -120 -90 -60 -30 0 30 60 90 120 150 180
Longitude [°]
240
235
230
225
220
215
210
205
200
195
190
185
180
175
170
165
L_S

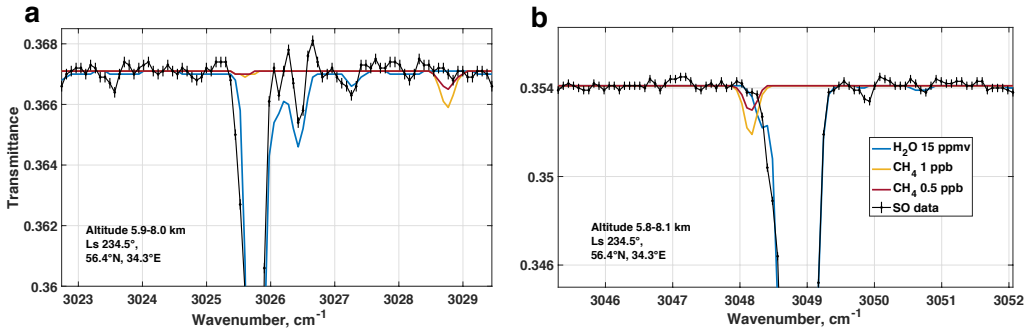
a
b
Transmittance
Altitude 5.9-8.0 km
Ls 234.5°,
56.4°N, 34.3°E
Wavenumber, cm-1
Altitude 5.8-8.1 km
Ls 234.5°,
56.4°N, 34.3°E
H2O 15 ppmv
CH4 1 ppb
CH4 0.5 ppb
SO data
Wavenumber, cm-1

555

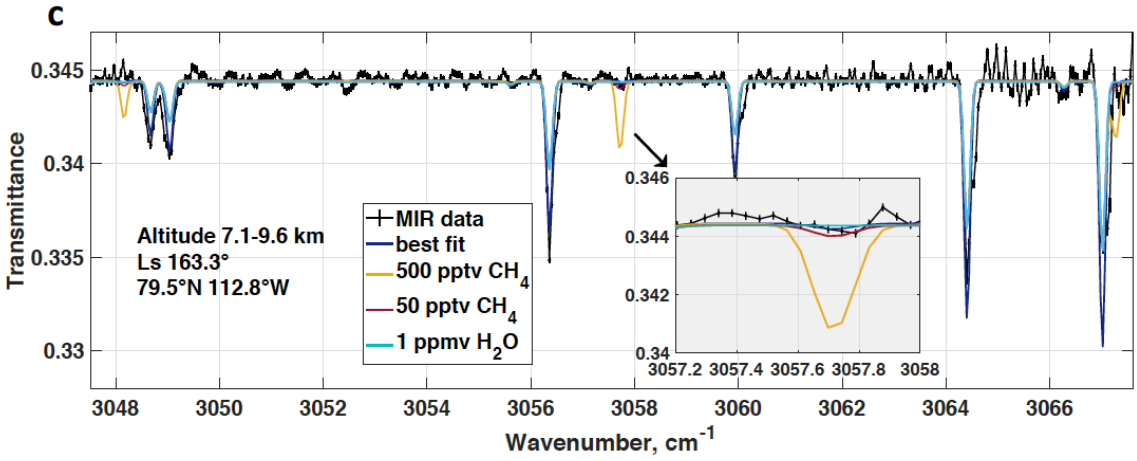
c
Transmittance
Altitude 7.1-9.6 km
Ls 163.3°
79.5°N 112.8°W
MIR data
best fit
500 pptv CH4
50 pptv CH4
1 ppmv H2O
Wavenumber, cm-1

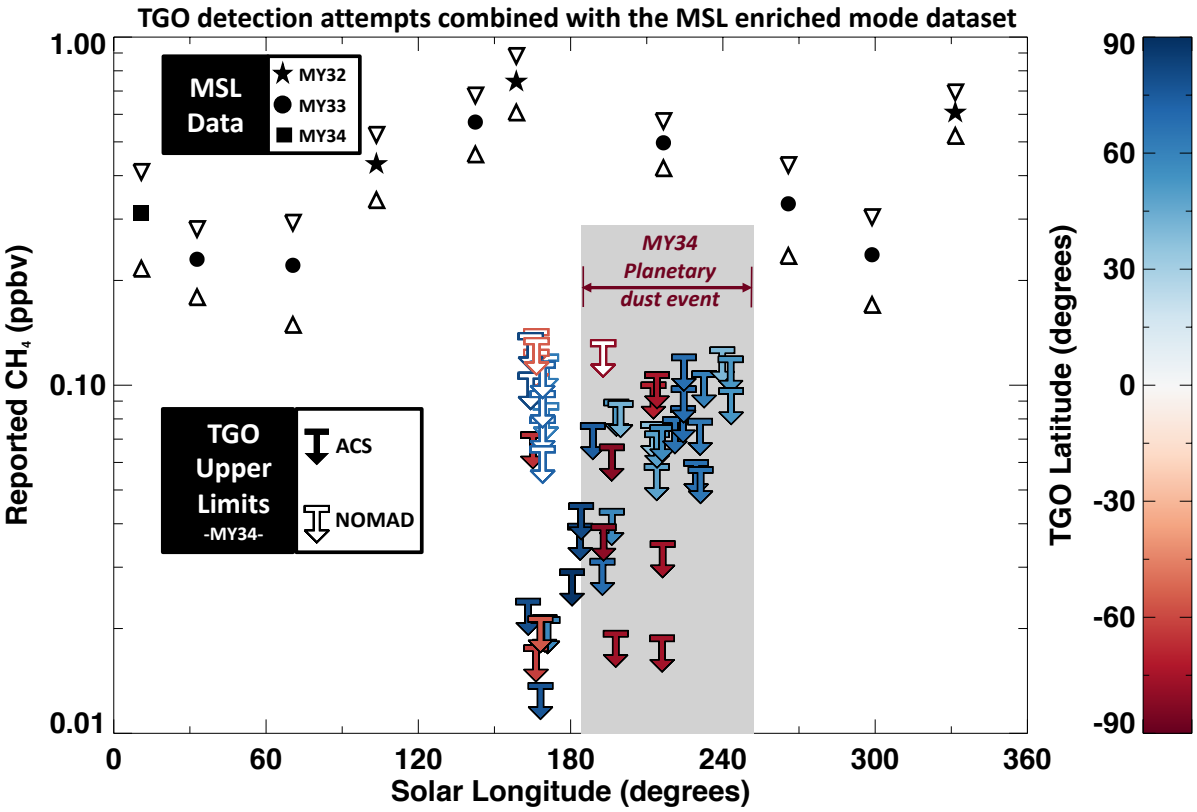
TGO detection attempts combined with the MSL enriched mode dataset
MSL Data
MY32
MY33
MY34
TGO Upper Limits
-MY34-
ACS
NOMAD
MY34 Planetary dust event
Reported CH4 (ppbv)
1.00
0.10
0.01
0
60
120
180
240
300
360
Solar Longitude (degrees)
TGO Latitude (degrees)
90
60
30
0
-30
-60
-90

560

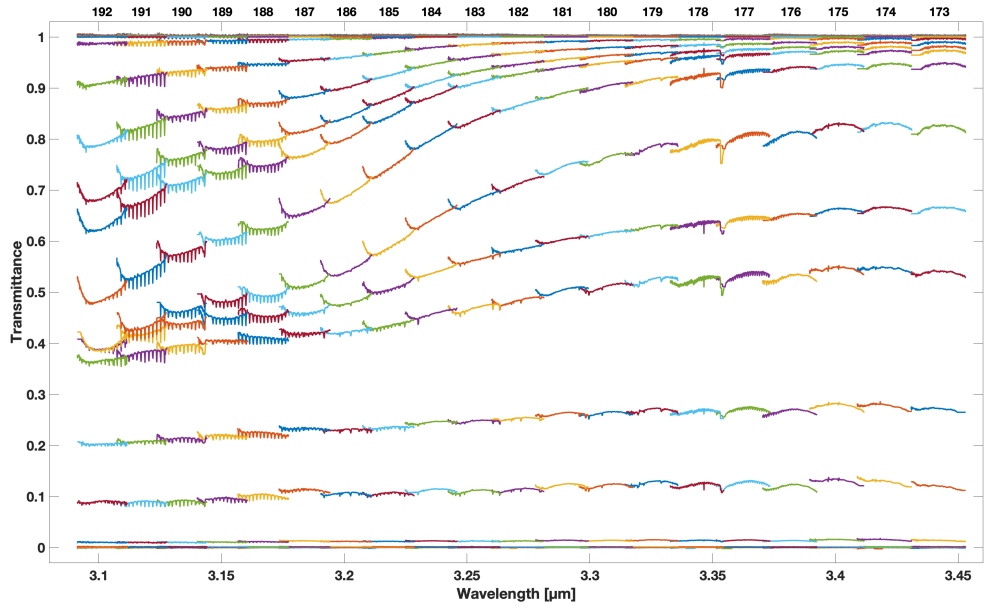
192 191 190 189 188 187 186 185 184 183 182 181 180 179 178 177 176 175 174 173
Transmittance
1
0.9
0.8
0.7
0.6
0.5
0.4
0.3
0.2
0.1
0
3.1 3.15 3.2 3.25 3.3 3.35 3.4 3.45
Wavelength [µm]

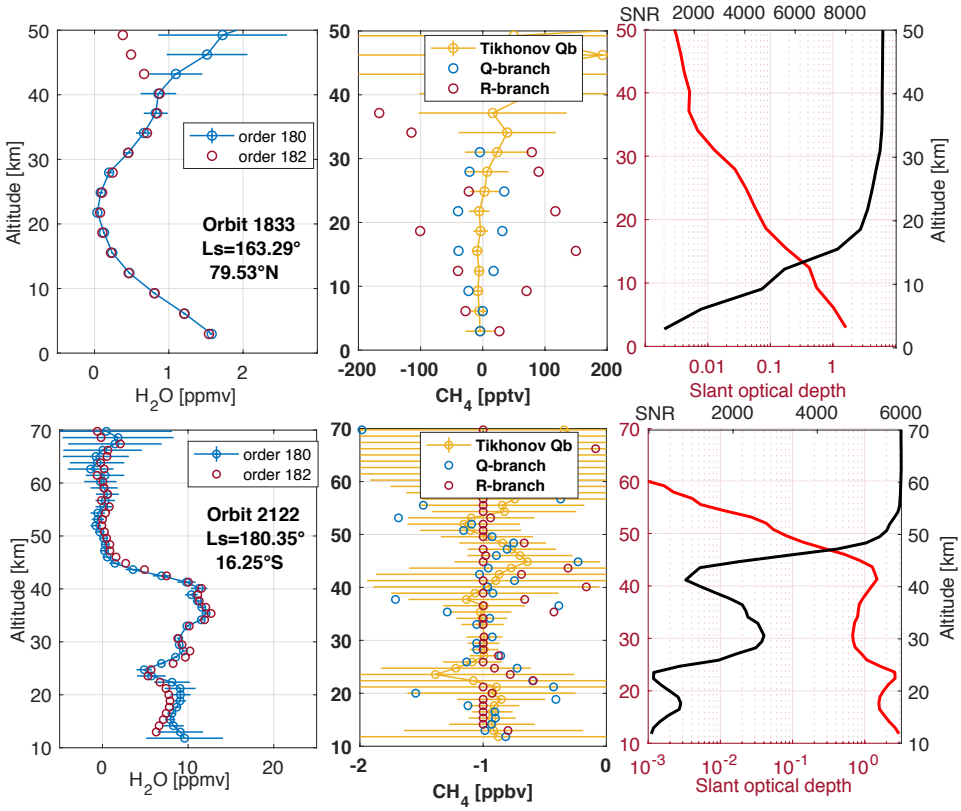
Altitude [km]
order 180
order 182
Orbit 1833
Ls=163.29°
79.53°N
H2O [ppmv]
Tikhonov Qb
Q-branch
R-branch
CH4 [pptv]
SNR 2000 4000 6000 8000
Slant optical depth
Orbit 2122
Ls=180.35°
16.25°S
H2O [ppmv]
CH4 [ppbv]
SNR 2000 4000 6000
Slant optical depth

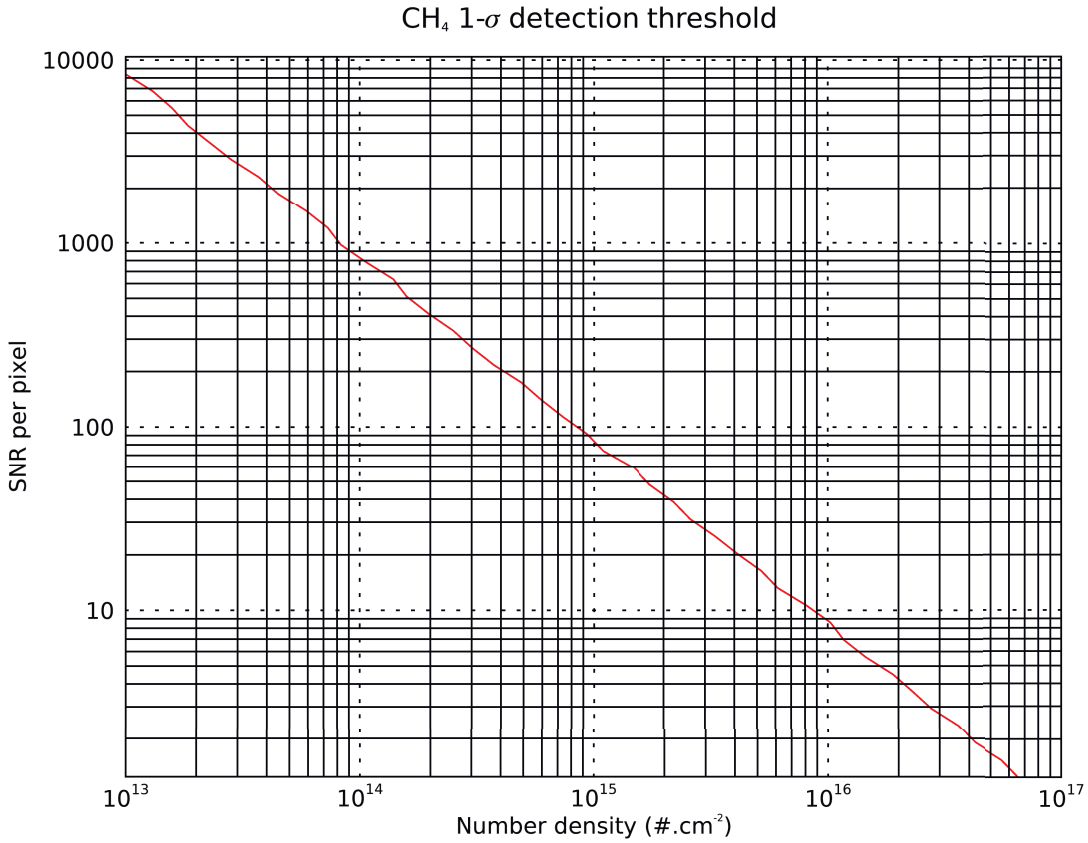
CH4 1-σ detection threshold
SNR per pixel
10000
1000
100
10
10^13
10^14
10^15
10^16
10^17
Number density (#.cm^-2)

565

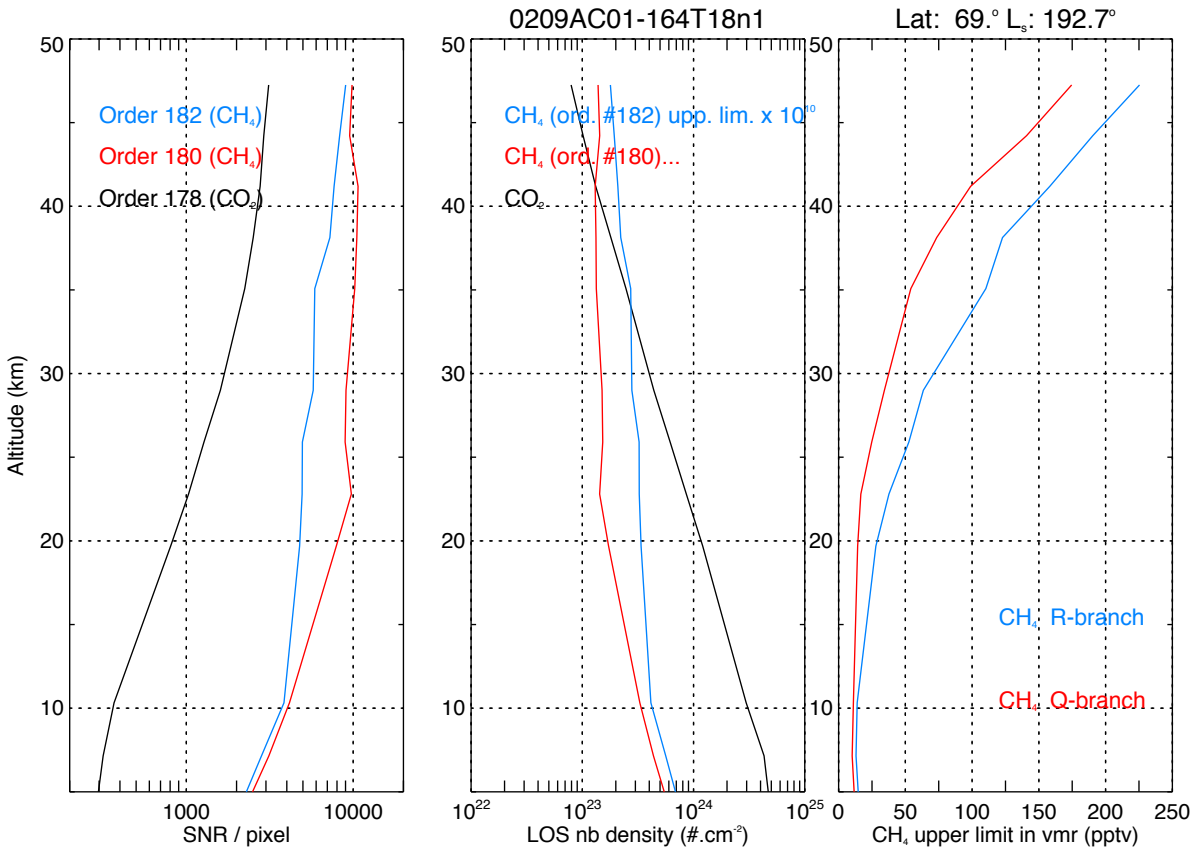
0209AC01-164T18n1
Lat: 69.° Ls: 192.7°
Order 182 (CH4)
Order 180 (CH4)
Order 178 (CO2)
CH4 (ord. #182) upp. lim. x 10^10
CH4 (ord. #180)...
CO2
CH4 R-branch
CH4 Q-branch
Altitude (km)
SNR / pixel
LOS nb density (#.cm^-2)
CH4 upper limit in vmr (pptv)

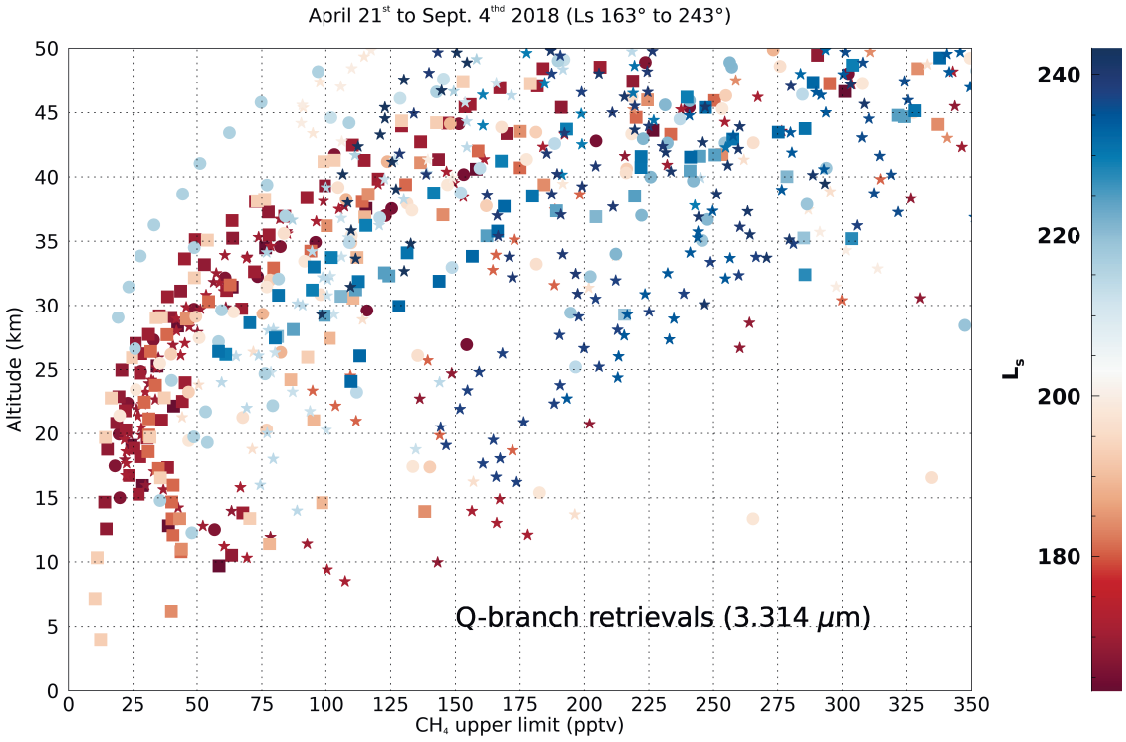
April 21st to Sept. 4thd 2018 (Ls 163° to 243°)
Altitude (km)
CH4 upper limit (pptv)
Q-branch retrievals (3.314 μm)
Ls
240
220
200
180

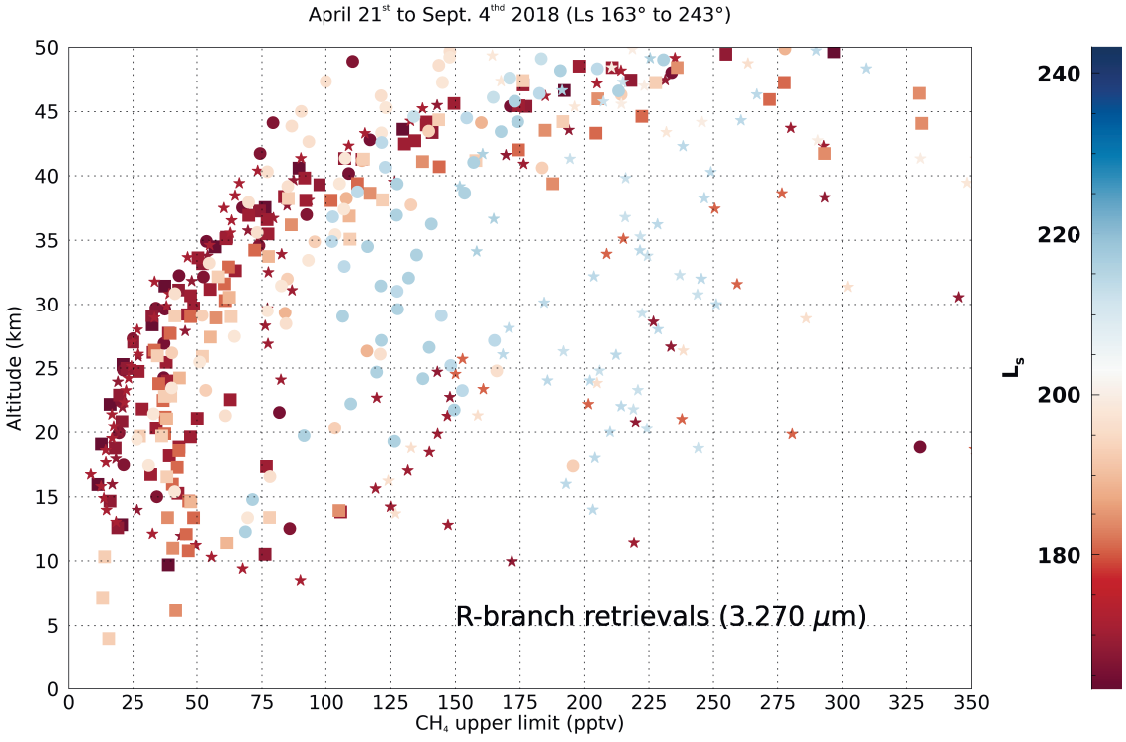
April 21st to Sept. 4thd 2018 (Ls 163° to 243°)
Altitude (km)
CH4 upper limit (pptv)
R-branch retrievals (3.270 μm)
Ls
240
220
200
180